Acta Geochim (2025) 44:945–961
https://doi.org/10.1007/s11631-025-00765-y

ORIGINAL ARTICLE

Carboniferous-Permian provenance shift in the southeastern Ordos Basin: Tracing early-stage uplift-erosion history of the western Qinling-Dabie orogen

Chuang Yang[1] · Jiaopeng Sun[1] · Zonglin Li[1] · Yukun Qi[1] · Kai Ye[1] · Junxiang Zhang[1] · Zhigang Wang[1]

Received: 5 November 2024 / Revised: 12 January 2025 / Accepted: 23 January 2025 / Published online: 13 February 2025

Abstract An enhanced understanding of the history of the western Qinling-Dabie orogen is pivotal in reconstructing geological processes of the east Asian mainland. However, less attention has been paid to its early-stage uplift-erosion history after closure of surrounding oceanic basins at the mid-Paleozoic. In this study, we undertook a comprehensive study including paleocurrent reconstruction, sandstone petrology, and detrital zircon U–Pb dating on Late Carboniferous to Early Permian successions in the southern Ordos neighboring the northern Qinling-Dabie. New provenance data reveal a significant provenance shift at the Carboniferous-Permian transition. The older Benxi Formation was sourced southerly from the North Qinling Terrane that provided detritus mostly of Neoproterozoic and Early Paleozoic ages. In contrast, Early Permian samples yield age relation dominated by Neoarchean, Paleoproterozoic, Early Paleozoic, and Late Paleozoic age populations, with a significant gap of ca. 1600–550 Ma, implying a sediment derivation from the Inner Mongolia Continental Arc. This shift is further verified by paleocurrent transition from south to north then. We suggest that the North Qinling Terrane experienced a significant uplift history from ca. 500 Ma and remained as a highland until end-Carboniferous. From Early Permian, the North Qinling Terrane was submerged, covered by widespread deltaic sedimentation there. Northerly source from the Inner Mongolia Continental Arc began to be accumulated in the northern flank of the North Qinling Terrane, before termination approximately along the southern North Qinling Terrane, where shallow-water carbonate shelf sedimentation sustained from Devonian to Triassic. This new finding indicates that uplift of the North Qinling Terrane lasted about 150 Ma after the Proto-Tethys Ocean closure.

Keywords Carboniferous-Permian transition · Provenance shift · Southern Ordos · Uplift history · Western Qinling-Dabie orogen

Supplementary Information The online version contains supplementary material available at https://doi.org/10.1007/s11631-025-00765-y.

✉ Jiaopeng Sun
sunjiaopeng@nwu.edu.cn

Chuang Yang
chenhuashengmi@sina.com

Zonglin Li
lizonglin96@163.com

Yukun Qi
qyk1005@163.com

Kai Ye
yekai20001010@sina.com

Junxiang Zhang
17318412486@163.com

Zhigang Wang
wangzhigang1126@sina.com

[1] State Key Laboratory of Continental Dynamics, Department of Geology, Northwest University, Northern Taibai Str. 229, Xi'an 710069, China

1 Introduction

Depicting the history of the construction and evolution of the Central China Orogenic System is a crucial and fundamental issue to understand the amalgamation history of the east Asian mainland and, therefore, has been the topic of intense studies for several decades (Zhang et al. 2001; Huang et al. 2018; Zhao et al. 2018). Most of these works focused on the geologic architecture, subduction-collision tectonism along the ancient ocean margins, and

Cenozoic to present intracontinental uplift (Dong et al. 2011, 2021; Dong and Santosh 2016; Richards 2015; Liu et al. 2021). However, controversy remains on the uplift-erosion history of the western Qinling-Dabie orogen at the central part of the Central China Orogenic System after intense mid-Paleozoic collision, due in part to the lack of conclusive thermal geochronological limits. At the transition from Proto-Tethys oceanic branch closure along the Shangdan and Erlangping sutures (Dong et al. 2011, 2021; Dong and Santosh 2016) to Paleo-Tethys Ocean closure along the Manlue suture farther south during the Silurian-Devonian (Sun et al. 2022), less attention has been paid to paleogeographic and tectonic evolution of the western part of the Qinling-Dabie orogen. This ambiguity has greatly hampered our understanding of the depositional history of the Ordos Basin and paleogeographic relation between the Ordos Basin and the south Qinling carbonate shelf. In particular, most recent studies prefer to regard the Ordos Basin as paleogeographically isolated from the Mianlue Ocean, separated by highland stretching the North Qinling (Li et al. 2021a).

Most ancient basins, where the original basin-source relation of which may no longer exist (Dickinson and Suczek 1979; Sun et al. 2020), have experienced multiple stages of uplift and subsidence cycles. The once-existing highlands may have been deeply eroded. Hence, many uncertainties exist in directly reconstructing the ancient basin-range framework (Dickinson and Suczek 1979; Dickinson 1985; Yang et al. 2014a, 2016). Yet, sedimentary records, fed by detritus from the nearby highland, deposited in sags adjacent to the orogen may preserve more complete clues on the deeply eroded orogen. The northwestern segment of the Qinling-Dabie orogen, represented by the North Qinling Terrane, is a deeply eroded orogen, as much of the North Qinling Terrane basement is now exposed to the surface, with limited Jurassic to present cover (Zhang et al. 2001; Dong et al. 2011; Dong and Santosh 2016), as a consequence of multiple-stage of uplift-subsidence history after its accretion onto the southern North China Bock at the mid-Paleozoic (Dong et al. 2018; Sun et al. 2022). Therefore, whether the North Qinling Terrane has been intensely uplifted after the mid-Paleozoic collision and how long did erosion of the orogen sustain are still unclear.

In this work, we conducted an integrated provenance study including paleocurrent reconstruction, sandstone petrology, and detrital zircon U–Pb geochronology on the Late Carboniferous to Early Permian successions in the southern Ordos that is located directly to the north of the North Qinling Terrane. Together with published geological approaches, we generate a new paleogeographic model on the southern Ordos- North Qinling Terrane. On the basis of this model, we provide a new estimate the erosion history of the North Qinling Terrane.

2 Geological background

2.1 Tectonic outline and geological setting

The North China Block bridges the Central China Orogenic System to the south and the Central Asian Orogenic System to the north (Fig. 1a), which are relics of the Tethys Ocean and Paleo-Asian Ocean, respectively (Dong et al. 2011, 2021; Xiao et al. 2015; Sun et al. 2024). On top of the North China Block basement to the north of the Jinning-Longhua fault, a NEE-trend zone of continental arc is known as the Inner Mongolia Continent Arc (Fig. 1b), construction of which was triggered by the Paleozoic to Triassic subduction and closure of the Solonker-Enger Us Ocean (Xiao et al. 2015; Sun et al. 2022, 2024; Song et al. 2023). Part of the southern North China Block was structurally involved in the rim of the Qinling-Dabie orogen during Mesozoic basin-ward thrusting of the orogen to the north (Fig. 2a; Dong and Santosh 2016; Dong et al. 2018). The Qinling-Dabie orogen is separated from the North and South China Blocks by the mid-Paleozoic Erlangping Suture and Triassic Mianlue Suture (Fig. 2a; Dong and Santosh 2016). It extends westward from the Tanlu Fault, via Dabie, Wudang, to Tongde (Dong and Santosh 2016), and can be further divided into two geologic units with distinct lithological assemblages and contrasting Precambrian geological histories, i.e., North and South Qinling Terranes, delineated by the Devonian Shangdan Suture (Zhang et al. 2001; Dong et al. 2011). The North Qinling Terrane is characterized by high-grade Archean to Paleoproterozoic basement rocks, which have been reworked by ca. 1000–940 Ma (peaking at ca. 950 Ma) and ca. 520–400 Ma (peaking at ca. 450 Ma) of plutonism and metamorphism (Dong et al. 2011; Sun et al. 2022) before Permian deltaic strata deposition. The South Qinling Terrane is dominated by a Neoproterozoic basement that was mostly formed ca. 850–680 Ma and was then covered by a nearly uninterrupted subdimension from Tonian to Triassic (Dong et al. 2012, 2011; Zhao et al. 2012; Sun et al. 2022). The Mesoproterozoic to present outcrops are widespread in the southern Ordos Basin along the Weibei Uplift, extending from Hejin in the east, via Tongchuan, Linyou, to Longxian in the west.

2.2 Carboniferous-Permian stratigraphy and paleogeography of the study area

The study area lies in the eastern portion of the Weibei Uplift, separated from the Qinling-Dabie Orogen by the Weihe Graben. Previous paleogeographic reconstructions have shown that sequences in the Weibei Uplift were accumulated in a vast depression of the Proto-Ordos Basin (Liu et al. 2009; Guo et al. 2019; Li et al. 2021a; Sun et al. 2024). At the Carboniferous to Permian, the North and South

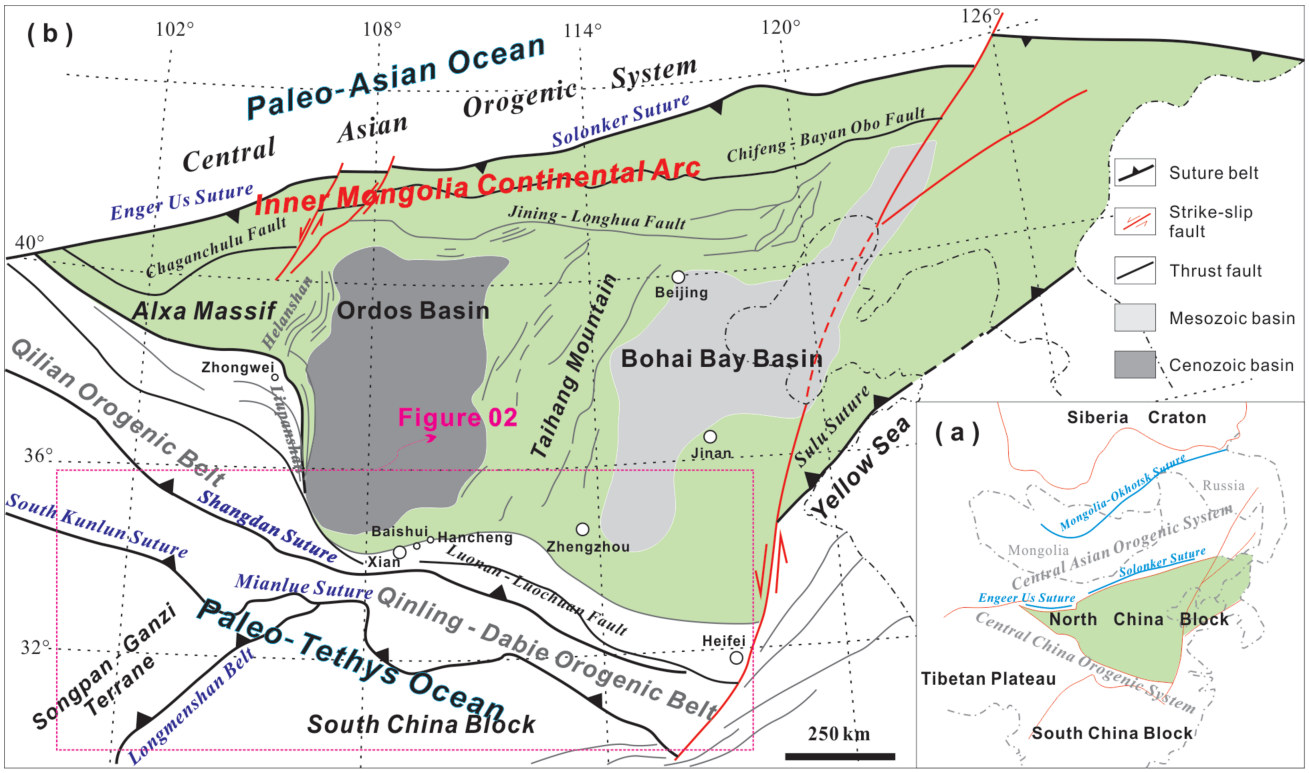

Fig. 1 Major structures of the North China Block. **a** Tectonic position of the North China Block in East Asia (modified from Meng et al. 2019); **b** adjacent tectonic elements of Ordos Basin (modified from Sun and Dong 2019)

Qinling Terranes were accreted onto the southern portion of the North China Block as its seaward margin, rimming the Mianlue Ocean of the northeastern limb of the Paleo-Tethys Ocean (Liu et al. 2015; Huang et al. 2018; Zhao et al. 2018). In contrast to the dominance of thick shallow-water carbonate successions in the South Qinling Terrane (Qian et al. 2015, 023), corresponding sequences are absent prior to deposition of the Benxi Formation at ca. 315 Ma in the southern North China Block and until deposition of the lower Shihezi Formation at ca. 290 Ma in the North Qinling (Dong and Santosh 2016; Li et al. 2021b, 2023; Shen et al. 2022).

Further to the north is the southern Ordos Basin, where an epeiric sea commenced at end-Carboniferous (Fig. 3a), represented by deposition of the Benxi Formation on top of thick bedded Ordovician carbonate rocks (Fig. 3b). The Benxi Formation is composed of tidal flat facies associations (Li et al. 2023), dominated by thick shale, mudstone interbedded with sandstone (Fig. 3c), having been inferred to be deposited in ca. 315–300 Ma (Wu et al. 2021). The Taiyuan Formation was accumulated in a short age span between 300 and 298 Ma (Yang et al. 2020), consisting of a lower unit of shale and mudstone and an upper part of bioclastic limestone (Fig. 3d, e; Li et al. 2021a, b; Peng and Guo 2023). The Shanxi Formation, with a stratigraphic age of ca. 298–295 Ma (Wu et al. 2021), is of deltaic facies (Zhu et al. 2008; Li et al. 2021a) composed mainly of thick bedded coarse-grained sandstone within coal-bearing mudstone (Fig. 3f). The Shihezi Formation is dominated by alternating sandstone and mudstone of various colors (Fig. 3g), having been interpreted to be accumulated at ca. 295–280 Ma (Wu et al. 2021) in a delta front sedimentary environment (Yu et al. 2017; Li et al. 2022). A sedimentary hiatus of ca. 280–260 Ma has been proposed to have occurred after the deposition of the Shihezi Formation (Wu et al. 2021; Shen et al. 2022), followed by the deposition of thick-layered fuchsia mudstone (Fig. 3h, i) alternating with grayish-red sandstone that indicates a seasonal lake environment (Sun et al. 2024). In summary, stratigraphy of the southern Ordos displays an upward shallowing sequence from a tidal flat-lagoon, via marine delta and nearshore, to a lake from Late Carboniferous to Early Permian.

3 Analytical methods

3.1 Paleocurrent, sandstone petrography, and modal composition

Analytical procedures for paleocurrent study and sandstone petrography followed standard procedures and

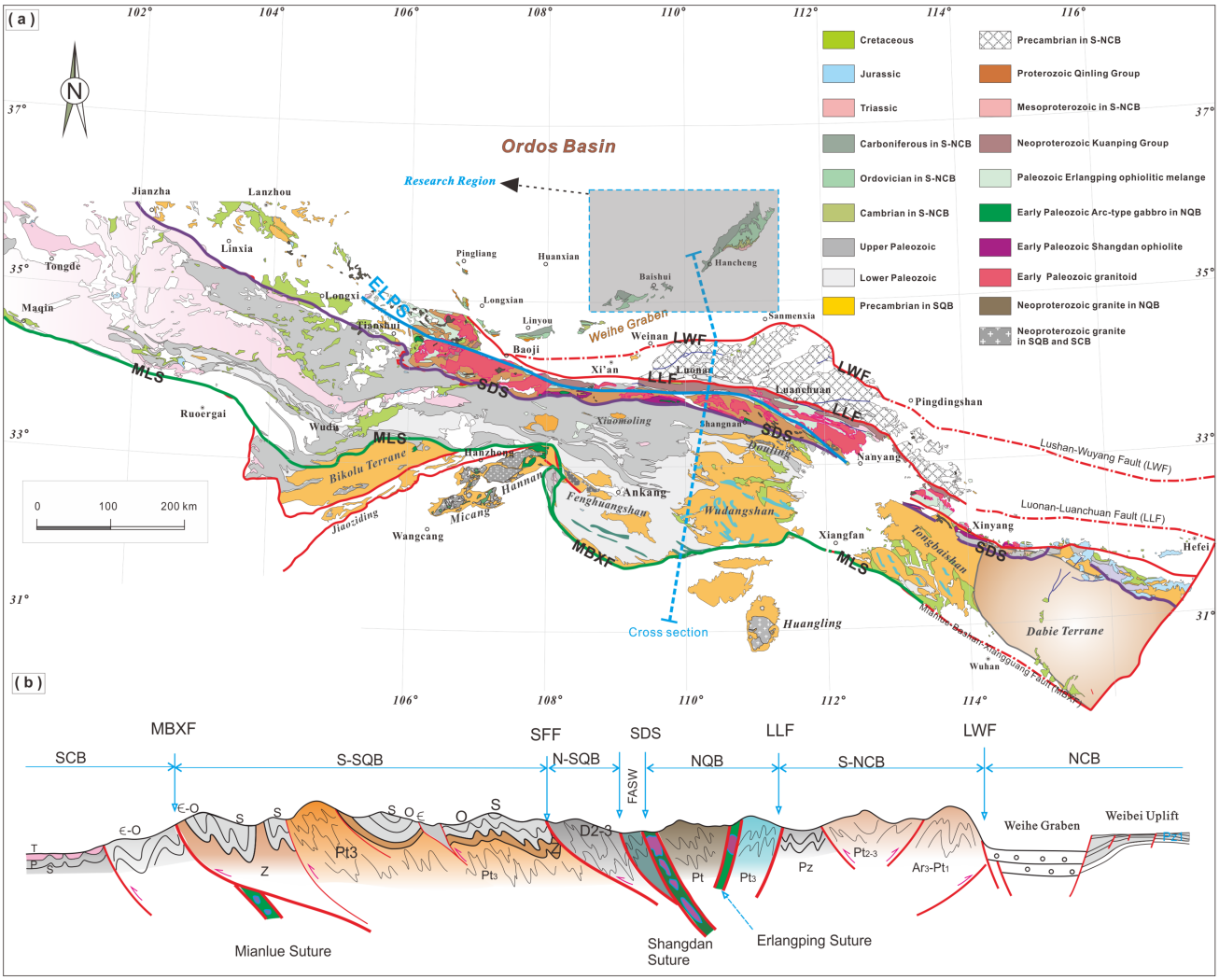

Fig. 2 **a** Tectonic overview map of the Qinling Orogenic Belt (modified from Dong et al. 2018). The solid lines in blue, purple, and green show the Erlangping suture, the Shangdan suture and the Mianlue suture, respectively. The red solid and broken lines represent major and blind faults, respectively; **b** cross-section (modified from Dong et al. 2018). NCB, North China Block; S-NCB, southern margin of NCB; NQB, north Qinling Belt; SQB, south Qinling Belt; N-/S-SQB, northern/southern parts of south Qinling Belt; SCB, South China block; LWF, Lushan-Wuyang fault; LLF, Luonan-Luanchuan fault; ELPS, Erlangping suture; SDS, Shangdan suture; MLS, Mianlue suture; SFF, Shanyang-Fengzhen fault; MBXF, Mianlue-Bashan-Xiangguang fault

related references that have been detailed in Sun et al. (2024). The peer-counting results and calculated modal composition data of 20 selected sandstone samples, along with parameters of principal grain types, are compiled in Supplementary Table 1. Representative photomicrographs are labeled in Fig. 4. For better clarifying distinction of major framework grains, modal composition data are plotted on Qt–F–L, Qm–Pl–K, and Lm–Lv–Ls diagrams of Fig. 5a–c. We also invoked the Qt–F–L and Qp–Lv–Ls (Fig. 5d, e) proposed by Dickinson and Suczek (1979) to interpret the tectonic settings of the source areas.

3.2 Zircon U–Pb geochronology

Each of the sandstone samples was sent to the Langfang Regional Geological Survey, China, using the conventional heavy liquid and magnetic techniques to separate the zircons. Under a binocular microscope, high-quality zircons were mounted in epoxy resin blocks. Then, the zircon was polished until it obtained a flat surface for the next step. Zircon cathodoluminescence imaging and U–Pb dating were conducted at the State Key Laboratory of Continental Dynamics, Northwest University, China. Zircons were dated in situ on a

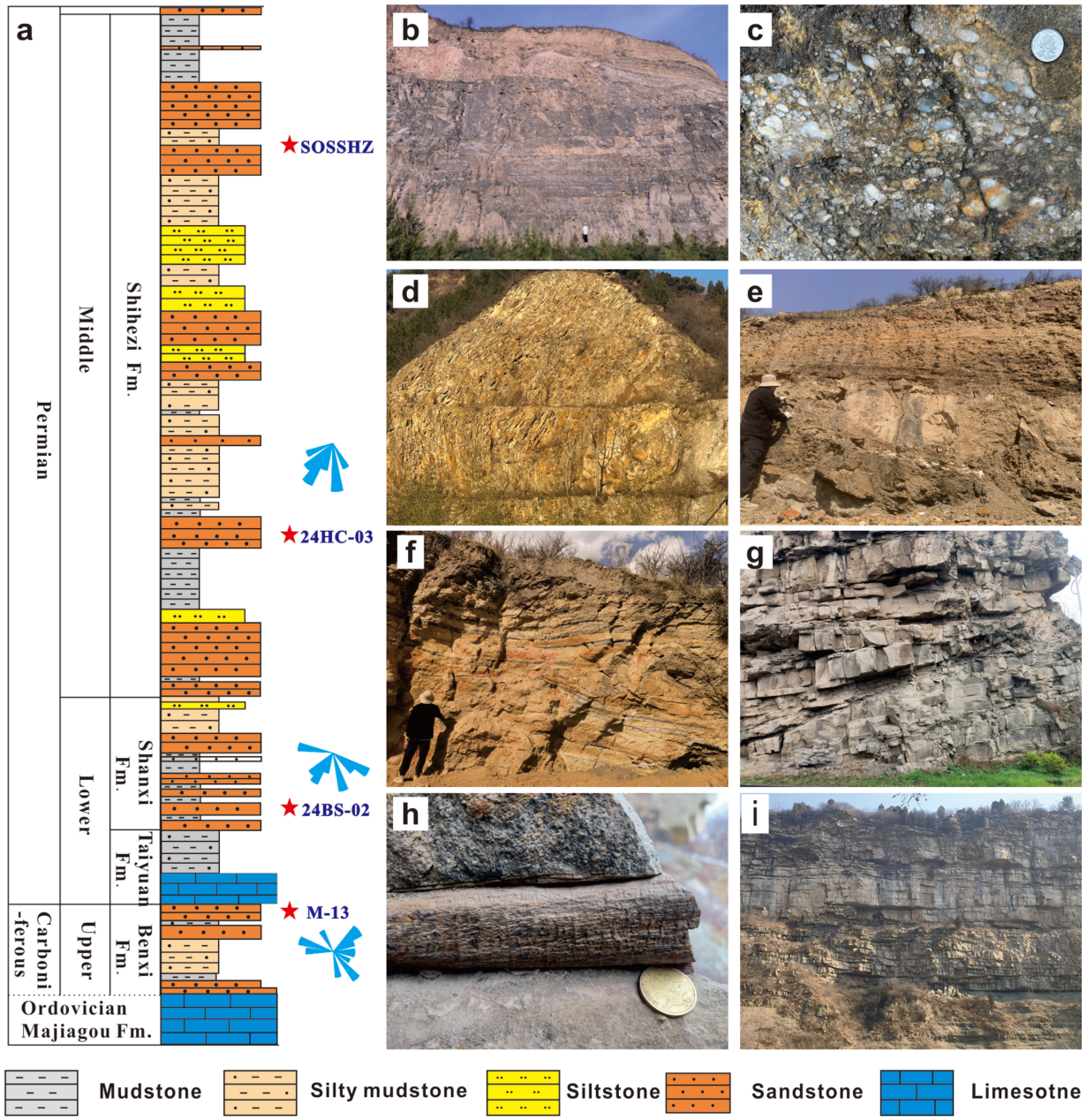

Fig. 3 **a** Upper Paleozoic lithostratigraphy of the basins in South Ordos Bain. Compiled from (Li et al. 2012) **b** Thick layer limestone of Majiagou Formation in Carboniferous. **c** quartz conglomerate of Benxi Formation at the top of Carboniferous; **d** Interbedded thin layer sandstone and mudstone of Taiyuan Formation; **e** Interlayered limestone of Taiyuan Formation; **f** Distribution characteristics of Shanxi Formation sand bodies in Baishui Section. **g** Superposed wedge sandstone in Shihezi Formation; **h** Horizontally distributed plant fossil in Shihezi Formation; **i** Sandstone of Shiqianfeng Formation without erosion

laser ablation instrument inductively coupled with a plasma mass spectrometer (LA–ICP–MS). The LA–ICP–MS was a GeoLas 200 M equipped with a 193 nm ArF excimer laser and a homogenizing and optical imaging system (MicroLas, Güttingen, Germany). Analyses were performed on an ELAN 6100 ICP–MS (PerkinElmer/SCIEX, Canada) with a dynamic reaction cell. The laser ablation spot size is about 30 μm, with a repetition rate of 10 Hz and energy of up to 90 mJ. GLITTER 4.0 (Macquarie University) software was used to calculate the $^{207}Pb/^{206}Pb$, $^{206}Pb/^{238}U$, $^{207}Pb/^{235}U$, and $^{208}Pb/^{232}Th$ ratios. The Harvard zircon 91500 was used as the external standard. The ages were computed by ISOPLOT 3.0 (Ludwig 2003). The detailed experimental procedures are shown in Liu et al. (2007). The Andersen (2002) method was used to make common Pb corrections. Age uncertainties are within a 90% confidence level. The $^{207}Pb/^{206}Pb$ ages were

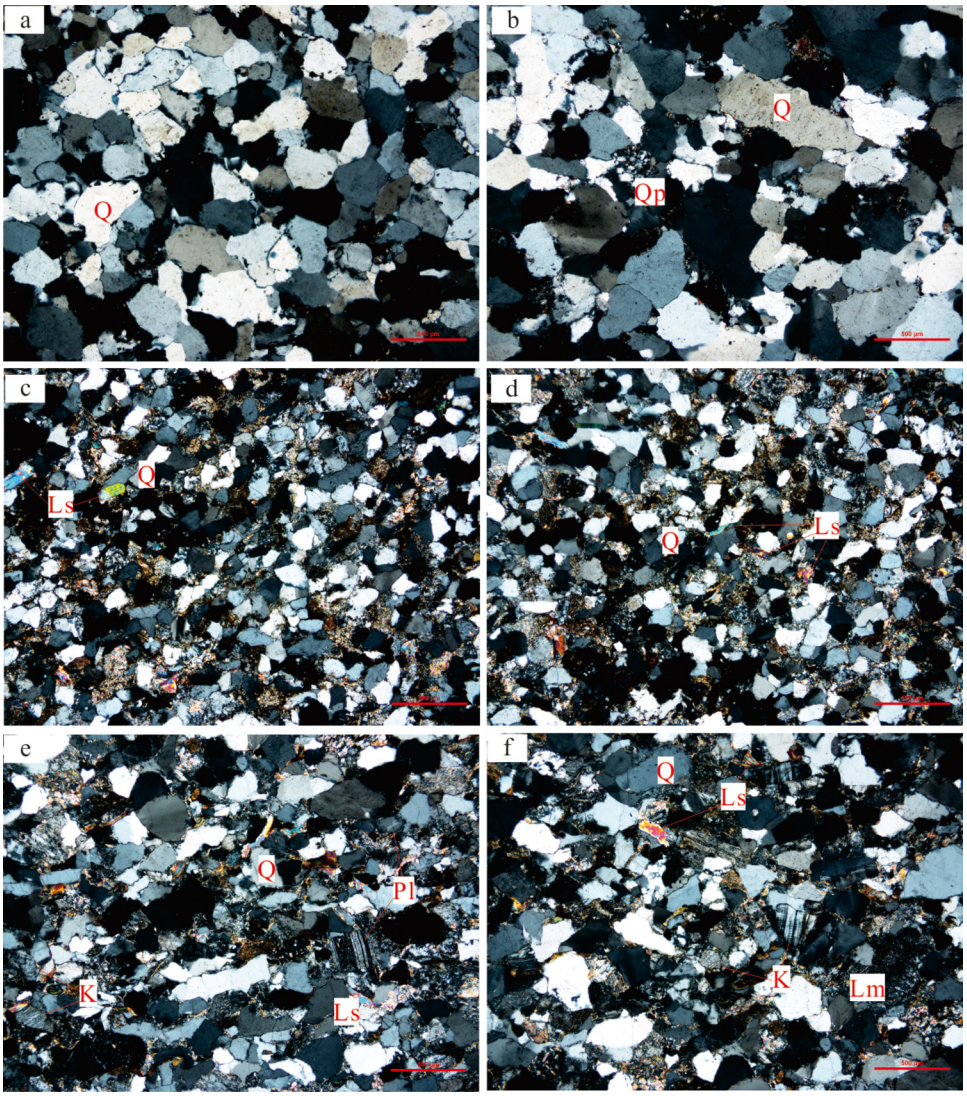

Fig. 4 Representative photomicrographs of sandstone from the Late Carboniferous-Permian strata **a**, **b** Benxi Fm; **c**, **d** Shanxi Fm; **e**, **f** Shihezi Fm. Abbreviations: Q-Quartz; Qp-Polycrystalline quartz; K-K-feldspar Pl-Plagioclase; Ls-Sedimentary rock fragments; Lm-Metamorphic rock fragments

chosen for grains older than 1000 Ma, and the $^{206}Pb/^{238}U$ ages were utilized for grains younger than 1000 Ma (Black et al. 2003). A full list of analytical results and trace elements of dated zircons are shown in Supplementary Tables 2 and 3, respectively. Representative cathodoluminescence (CL) images along with analytical numbers, Th/U ratios, and zircon U–Pb ages of dated zircon can be seen in Fig. 6. All data are plotted on U–Pb concordia diagrams, while only data with discordance < 10% are labeled in probability density distribution curves (Fig. 7) and are used for discussion (Fig. 8). Furthermore, the trace element data from detrital zircons provide valuable insights into the tectonic setting (Fig. 9) and facilitate the reconstruction of crustal thickness (Fig. 10). The methodology for reconstructing crustal thickness is based on the europium anomaly (Eu/Eu*) in detrital zircons, as detailed in Tang et al. (2021). After data synthesis, the chondrite-standardized $Eu/\sqrt{Sm \times Gd}$ values were calculated for zircons younger than 500 Ma to determine their Eu/Eu* values. These calculated values were then applied to the empirical equation $z = (84.2 \pm 9.2) \times Eu/Eu^* + (24.5 \pm 3.3)$ to estimate the crustal thickness z (in kilometers).

4 Results

4.1 Paleocurrent directions

We retrieved paleocurrent data by measuring orientations of gravel imbrications and large-scale plate- and trough-cross beddings preserved in thick- and massive-bedded sandstones of the Benxi, Shanxi, and Shihezi Formations. We prefer not to use data from paleocurrent indicators preserved in beds with thickness less than 0.5 m, as we are afraid that these beds may be generally formed by sedimentary rework of

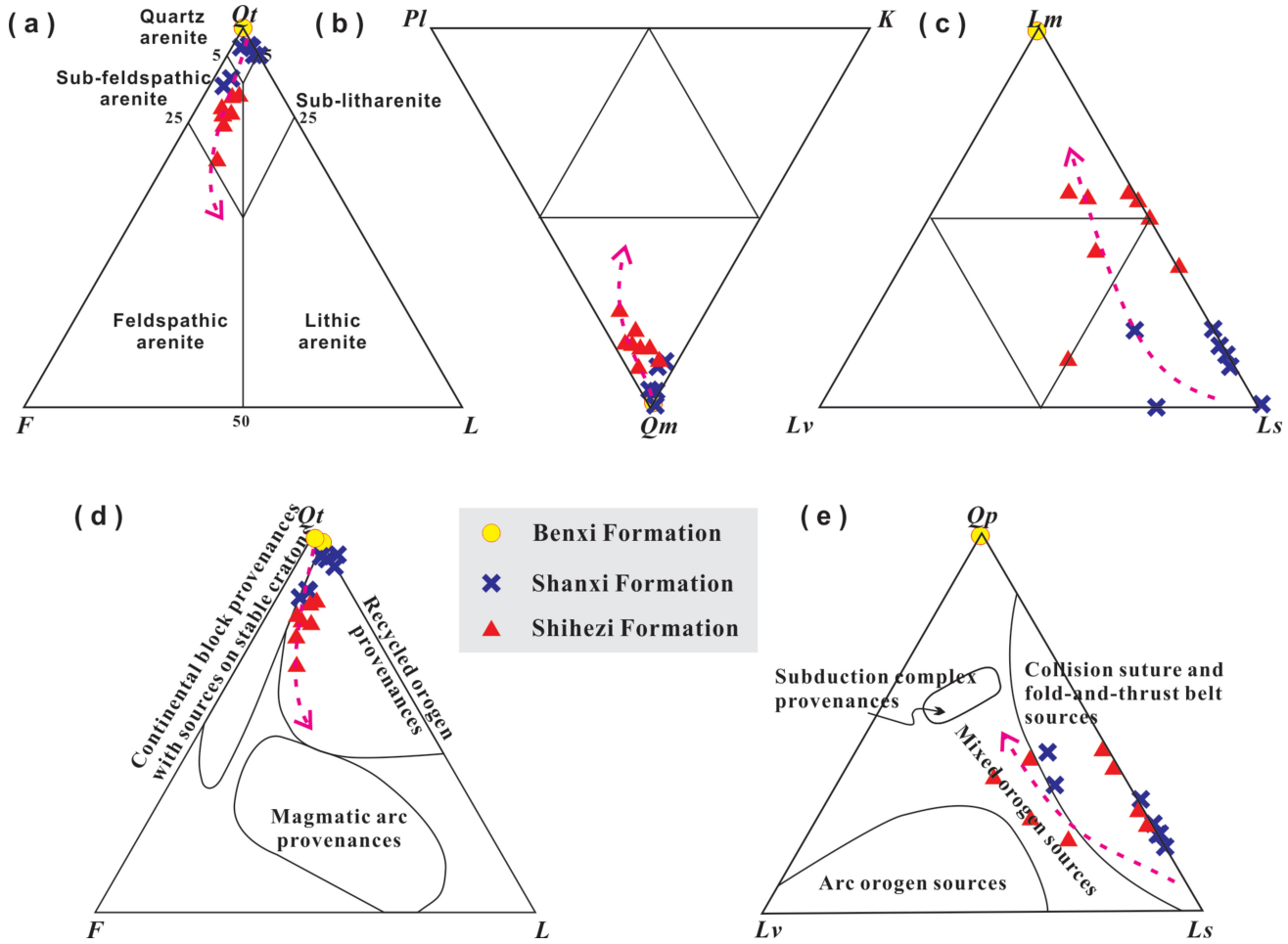

Fig. 5 Ternary plots for Late Carboniferous-Permian sandstone modal composition data from the central Ordos Basin. **a** Petrologic classification diagram according to (Pettijohn 1975). **b**, **c** Pl-K-Qm and Lv-Ls-Lm diagrams. **d**, **e** Provenance discrimination diagrams (Dickinson and Suczek 1979; Dickinson 1985). Abbreviations: Qt-total quartz (Qm + Qp); Qm-monocrystalline quartz; Qp-polycrystalline quartz; F-K-feldspar + plagioclase; L-lithic fragments; Lt–L + Qp; Lv-volcanic lithic fragments; Ls-sedimentary lithic fragments. Red arrows indicate the evolutionary trend

waves and tides, directions of which cannot be used to trace the position of sources.

The obtained data exemplified by rose diagrams indicate a change of source-to-sink in the southern Ordos (Fig. 3). Paleocurrent data of the Benxi Formation display complex patterns. The rose diagram for the Benxi Formation samples contains three groups of paleocurrent directions, i.e., northeastward, westward, and southward, but imply a dominantly north-northeastward paleoflow direction, while paleocurrent data of Early Permian Shanxi and Shihezi Formations are generally unidirectional. Paleocurrent data of the Shanxi Formation vary freely from 120° to 300°, while the rose diagram refers to a clear averaged direction of about 190° that implies a south-southward flowing deltaic system then. Paleocurrent data from the Shihezi Formation are consistently southward-directed, varying slightly from about 160° to 230°, with most results concentrating at about 210°. The paleocurrent data suggest that sediment deviation of the Shanxi and Shihezi Formations were from the north.

4.2 Petrographic data

The petrologic signatures of sandstones from Late Carboniferous to Early Permian successions fall into two mutually exclusive categories (Fig. 5). Samples of the Benxi Formation are all quartz arenite, with dominance of monocrystalline quartz (92%–95%) and a rare amount of polycrystalline quartz (5%–8%). Samples of the Shanxi Formation and Shihezi Formation are mostly sub-feldspathic arenite, with some of the Shanxi Formation samples falling in the field of quartz arenite (Fig. 5a). Monocrystalline quartz is predominant in all samples, ranging from 62% to 94% (Fig. 5b). Feldspar accounts for 1%–22% of all grains, including plagioclase feldspar

Fig. 6 Representative cathodoluminescence (CL) images of detrital zircons, showing the LA–ICP–MS analytical spots for U–Pb isotope spots and corresponding ages

(0%–17%) and K-feldspar (0–7%). Lithic fragments make up 4%–17% of all grains, comprising mainly 1%–5% of metamorphic lithics and 3%–7% of metamorphic lithic fragments. Almost no volcanic lithic fragments were found.

Average compositions of sandstones from the Benxi Formation are %Qt, F, L = 98, 0, 1; %Qm, Pl, K = 93, 0, 0; and %Qp, Lv, Ls = 0, 0, 0. These compositions all fall within the stable craton interior provenance field (Fig. 5e) of Dickinson (1985). Average sandstone framework compositions for the Shanxi Formation samples are %Qt, F, L = 91, 3;, 7 and %Qp, Lv, Lm = 2, 0, 1. Average sandstone framework compositions for the Shihezi Formation samples are %Qt, F, L = 78, 14, 8 and %Qp, Lv, Lm = 2, 1, 4. These are plotted in the recycled orogen and stable craton provenance fields in the Qt–F–L diagram (Fig. 5e) and in the collision suture, fold-and-thrust belt, and mixed orogen sources in the Qp–Lv–Ls diagram (Fig. 5f). A clear compositionally immature trend can be viewed in all diagrams, presented by an increasing amount of feldspar and lithic fragment grains.

4.3 LA–ICP–MS zircon U–Pb dating

Four representative medium- to coarse-grained sandstone samples were selected for zircon U–Pb dating by LA–ICP–MS spectrometry. Of these three sandstone samples, sample M-13 is from the Benxi Formation, sample 24BS-02 is from the Shanxi Formation, sample 24HC-03 is from the lower Shihezi Formation, and sample SOSSHZ from the upper Shihezi Formation. Approximate geologic locations and stratigraphic levels of these samples from this and published studies are shown in Fig. 3.

Zircons from the Benxi Formation sample M-13 are well rounded and sorted with clear margins of abrasion. Diameters of unbroken grains range from 70 to 120 μm (Fig. 6a). Most zircons show clear oscillatory zoning and nebulous internal structures, with a few grains being sector zoned or structureless. A total of 100 analyses on 100 grains produced 98 ages with sufficient precision for geochronological interpretation. Most analyses are concordant; the ages range from 495 to 423 Ma (34 grains), from

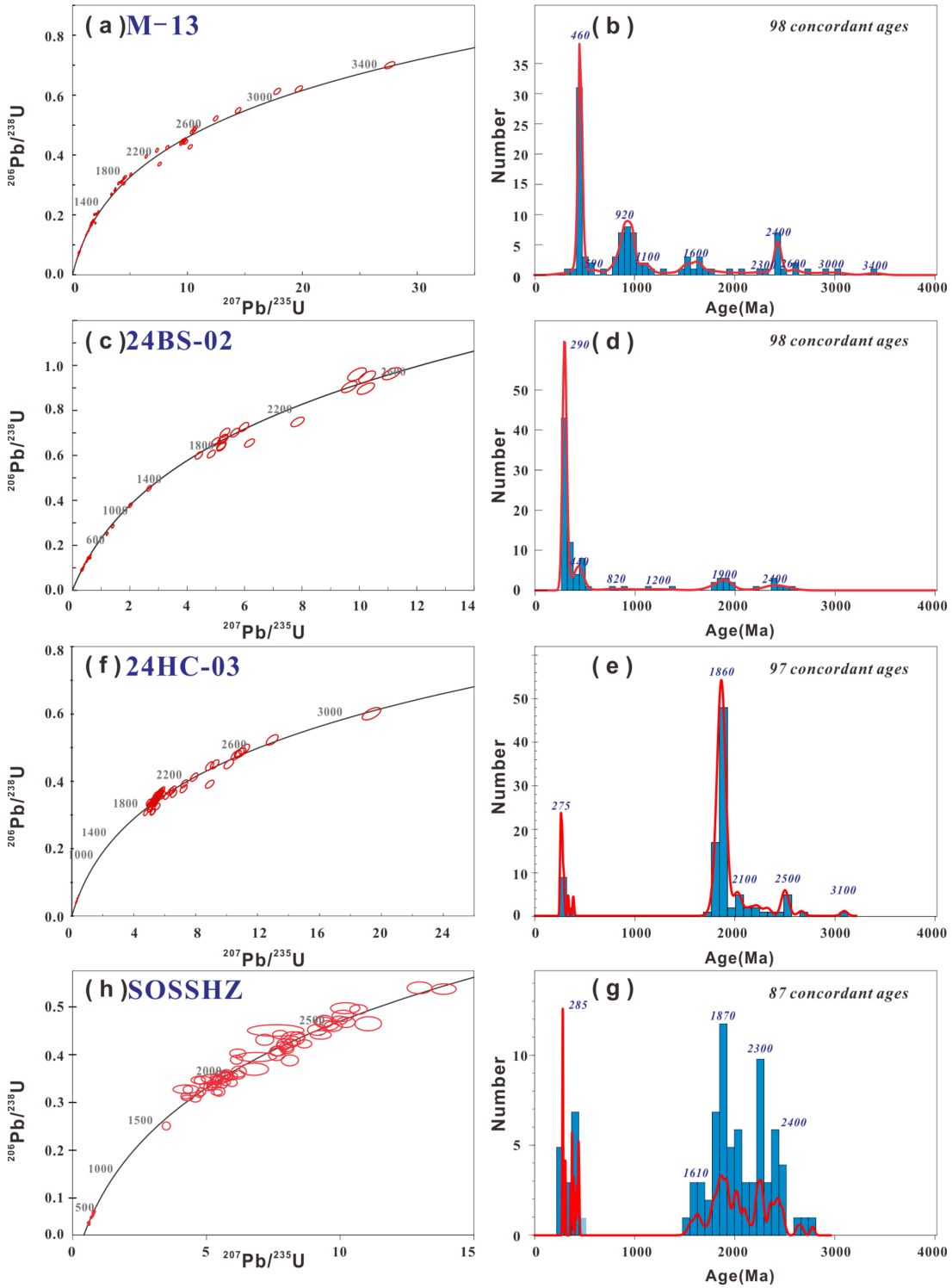

Fig. 7 U–Pb concordia diagrams, frequency (bars), and probability density distribution (curves) of ages showing the results of laser ablation inductively coupled plasma mass spectrometry U–Pb dating of the detrital zircons from the Benxi, Shanxi, and Shihezi Formations

1034 to 883 Ma (20 grains), from 1793 to 1512 Ma (9 grains), and from 2595 to 2238 Ma (13 grains) (Fig. 7a, b).

Sample 24BS-02 was collected from medium- to coarse-grained sandstone layers in the lower portion of the Shanxi Formation. Zircons in the samples range from 80 to 140 μm in length, ranging from colorless and euhedral crystals to well-rounded and highly spherical grains (Fig. 6b). Up to 98 of 100 analyses are concordant, ranging

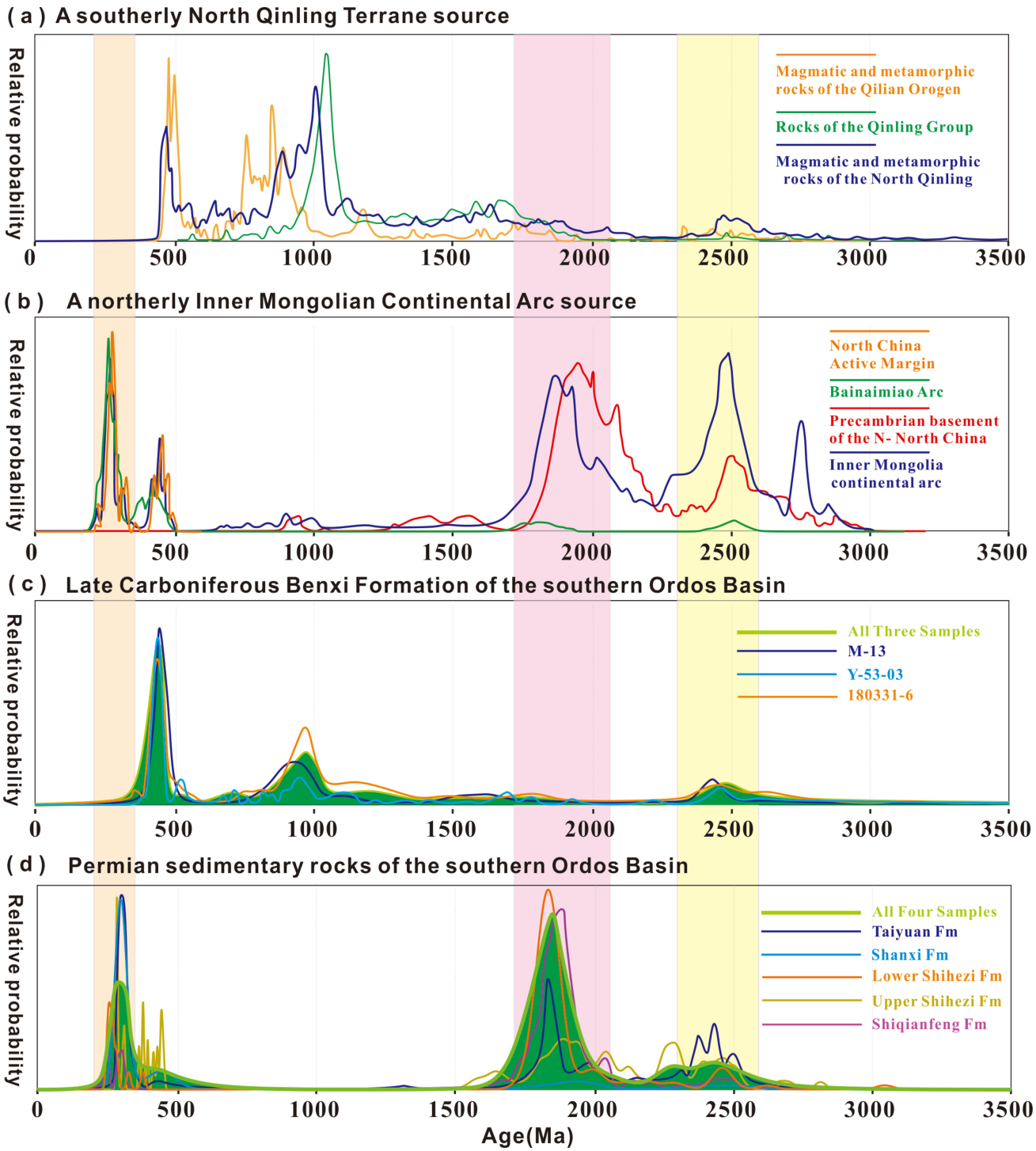

Fig. 8 Probability density distribution (curves) of ages for **a** a southerly Qinling source: magmatic and metamorphic rocks of the Qilian Orogen (Zhang et al. 2015), rocks of the Qinling Group (Sun and Dong 2020), magmatic and metamorphic rocks of the North Qinling (Sun and Dong 2020); **b** a northerly Inner Mongolia Continental Arc source: North China active margin, Bainaimiao Arc and North China Block (Eizenhöfer and Zhao, 2017), Precambrian basement of the northern North China Block (Zhang et al. 2016a, b; Xu et al. 2017), North China Arc (Wang et al. 2015), Inner Mongolia Continental Arc (Sun et al. 2024); **c** sandstones from the Late Carboniferous in the Ordos Basin (zircon data from Zhang 2020; Sun 2019); **d** sandstones from the Early Permian in the Ordos Basin. Zircon data of the Taiyuan Formation come from Li et al. (2023); data of the Shiqianfeng Formation come from Wang et al. (2023)

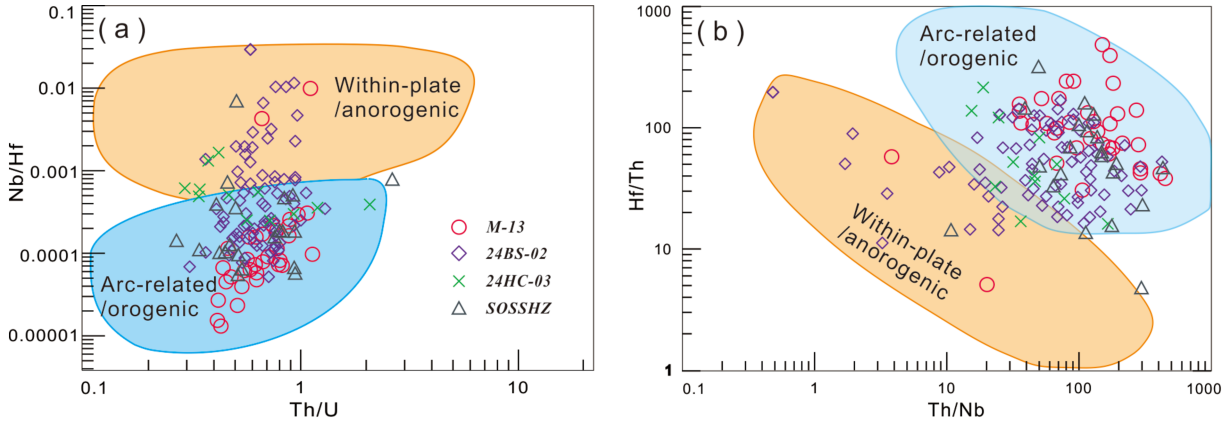

Fig. 9 Th/U vs. Nb/Hf and Th/Nb vs. Hf/Th diagrams for detrital zircons from the Late Carboniferous to Permian sediments in the central Ordos Basin (Base cited from Hawkesworth and Kemp 2006)

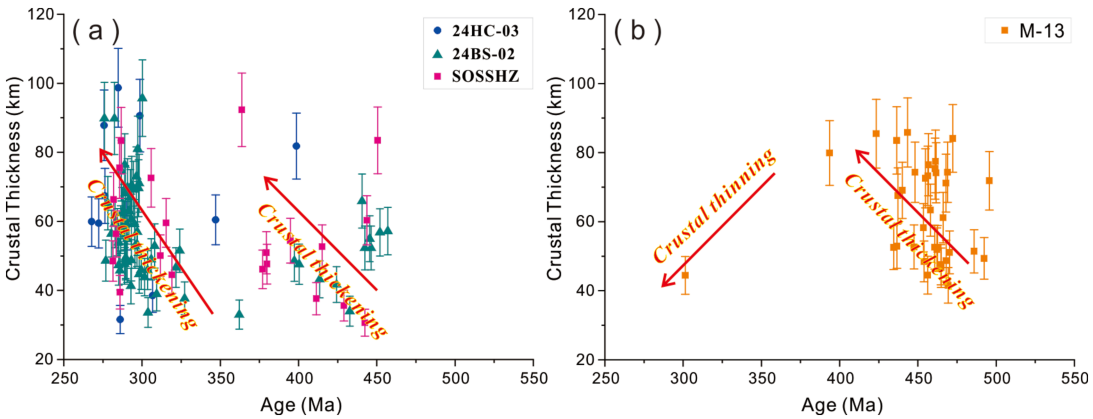

Fig. 10 Provenance crustal thickness evolution of the Ordos Basin and North China Block, reconstructed from Eu/Eu* in detrital zircons. The method for crustal thickness calculation was according to Tang et al. (2021)

widely from ca. 2600 to 276 Ma. The Paleozoic age components are predominant, with 67 ages of 276–457 Ma constituting the largest concentration, with an age peak at ca. 290 Ma. Two secondary age clusters occur in ca. 1.7–1.9 Ga ($n = 10$) and ca. 2.2–2.5 Ga ($n = 7$) (Fig. 7c, d).

A total of 100 analyses on lower Shihezi Formation sandstone 24HC-03 collected yielded 97 reliable ages with discordance of less than 10% (Fig. 7e, f). The notable age cluster occurs at ca. 1860 Ma, with secondary age peaks at ca. 275 and 2500 Ma (Fig. 7c). The sample from upper Shihezi Formation sandstone SOSSHZ displays a detrital zircon U–Pb age relation, defined by 87 concordant ages (Fig. 7g, h), which is similar to that of the sandstone 24HC-03, dominated by Archean to Paleoproterozoic ages with two separated age peaks at ca. 1870 and 2300 Ma. A total of 17 zircons have ages of Paleozoic, defining a youngest age peak of 285 Ma. A notable age gap between 1600 and 600 Ma can be found.

In summary, the Late Carboniferous and Early Permian sandstones have different detrital zircon U–Pb age patterns (Fig. 8), reflected by observation that common ages of ca. 1000–800 Ma in the Late Carboniferous sandstones are absent in Early Permian samples and that common age components of ca. 320–280 Ma in the Early Permian sandstones are absent in Late Carboniferous samples.

Trace element analyses reveal that the analyzed detrital zircons exhibit averaged Hf > 8000 ppm and averaged Nb < 170 ppm, consistent with derivation from a granitic protolith with SiO_2 content lower than 75% (Belousova et al. 2002). The resulted Th/U ratios fall within a narrow span of 0.2–1, whereas the Nb/Hf values range widely from 0.00001 to 0.01 (Fig. 9a). The Th/Nb and Hf/Th ratios scatter widely in 1–600 and 10–800 (Fig. 9b), respectively. The Eu/Eu* values calculated for Late Carboniferous and Early Permian samples indicate distinct differences in crustal thickness (Fig. 10). The Permian samples have Sm content

of 0.67–125.65 ppm (averaged 8.29 ppm), Eu content of 0.04–33.78 ppm (averaged 1.72 ppm), and Gd content of 3.36–464.61 ppm (averaged 31.27 ppm). The resulting Eu/Eu* values for Permian samples range from 0.02 to 0.95, showing two increasing trends with ages from ca. 460 to ca. 390 Ma and ca. 320 to ca. 280 Ma. The Carboniferous samples have Sm content of 0.23–109.5 ppm (averaged 4.13 ppm), Eu content of 0.04–4.04 ppm (averaged 0.53 ppm), and Gd content of 1.49–114.5 ppm (averaged 14.9 ppm). These samples exhibit Eu/Eu* values ranging from 0.02 to 1.15, characterized by an increase–decrease pattern peaking at ca. 390 Ma. Reconstruction of crustal thickness based on Eu/Eu* calculations reveals that the Inner Mongolia Continental Arc experienced thickening to about 60 km at ca. 440–400 Ma, followed by thinning to about 30–40 km at ca. 370–330 Ma, and renewed thickening to about 60 km at ca. 280 Ma (Fig. 10a). The North Qinling Terrane crust increased in thickness from ~ 43 to ~ 65 km during ca. 500–390 Ma, before thinning to ~ 40 km at ca. 300 Ma (Fig. 10b).

5 Discussion

5.1 Evolving sedimentary provenances at Carboniferous-Permian transition

Sandstones of the Benxi Formation are mostly quartz arenites, with dominance of quartz grains, although morphologies of quartz grains are irregular (Fig. 5a, b). In contrast, sandstones from the Taiyuan, Shanxi, and Shihezi Formations are mostly lithic arenite or sublitharenite, characterized by enrichment of lithic fragments and paucity of feldspar grains. The difference in petrology can also be viewed from the tectonic discrimination diagram, considering that the Permian samples generally fall into mixed sources including craton basement, arc orogen, and collision belt (Fig. 5). For samples of this study, the detrital zircon U–Pb age spectrum for the Benxi Formation is rather distinct from those for the overlying Shanxi and Shihezi Formations, exemplified by the presence of a Neoproterozoic age cluster and the absence of Late Carboniferous age cluster (Figs. 7, 8). Furthermore, Th/U versus Nb/Hf and Th/Nb versus Hf/Th discrimination diagrams unveil an arc-related and orogenic tectonic background (Fig. 9), in which detrital materials of our Early Permian samples were eroded and accumulated (Hawkesworth and Kemp 2006).

We compiled detrital zircon U–Pb samples from the Benxi, Taiyuan, Shanxi, and Shihezi Formations in the southern Ordos (Fig. 8). The Benxi Formation samples are characterized by the presence of ca. 900 Ma age clusters, which are commonly absent from the overlying Permian successions, defining a significant provenance shift that occurred during the transition of the deposition of Benxi and Taiyuan Formation at ca. 300 Ma. The change in provenance can be further verified by the contrasting paleoflow directions, as the Benxi Formation displays north-flowing results, whereas data from the Shanxi and Shihezi Formations are south-directed (Fig. 3).

For potential source areas, first, we must highlight that much of the western North China Block was inundated by a vast basin that stretched from the southern Inner Mongolia Continental Arc to the northern Qinling (Chen et al. 1989; Li et al. 2012; Shao et al. 2015), precluding the possibility of sediment injection from the western North China Block basement and covers. Hence, the Inner Mongolia Continental Arc and the Qinling orogen should be the only two candidates (Fig. 8a, b), consistent with the fact that in both regions, the Carboniferous to Permian deposits are thinner or even absent (Yang et al. 2014b, 2021; Sun et al. 2020; Dong et al. 2021).

For the Benxi Formation, a southerly provenance is observed. Paleogeographic reconstructions show that during the Late Carboniferous to Early Permian to the south of Pingliang–Linyou–Hejin, there was no sedimentation (Guo et al. 2019; Li et al. 2023), supported by the fact that the Permian Shanxi or Shihezi Formations directly cover pre-Silurian units in Pingliang (Sun et al. 2020) and Luonan (Yang et al. 2018, 2021). The southern margin of highland extends to the north of Shangdan Suture, considering that thick shallow carbonate shelf depositions sustained from Devonian to Triassic (Yu and Meng 1995) throughout the South Qinling. Hence, the source area covered the North Qinling Terrane and southern North China Block, where bed rocks jointly provide suitable detritus for the Benxi Formation (Fig. 8a, c). The oldest age population of ca. 2600–2400 Ma could be attributed to the basement rocks of either the north Qinling Terrane or the southern North China Block. We prefer the former as a more likely candidate, because the common tectonic units formed at ca. 2000–1800 Ma in the southern North China Block (Zhao et al. 2012; Dong and Santosh 2016) are not substantial. However, this phenomenon is common in samples from the North Qinling Terrane basement (Fig. 8a; Sun et al. 2022). The major age concentrations of ca. 1000–800 Ma and ca. 550–400 Ma match well with two major tectonic events in the North Qinling Terrane (Fig. 8c; Dong and Santosh 2016; Sun et al. 2024). The ca. 1000–800 Ma imprints have been related to the Rodina supercontinent assemblage, exemplified by voluminous S-type plutonism peaking at ca. 900 Ma and a small amount of ca. 750 Ma mafic dikes (Dong et al. 2021). The ca. 550–400 Ma tectonism identified in the North Qinling Terrane has been explained to be a consequence of subduction-closure of the Shangdan Ocean and the Erlangping back-basin (Dong et al. 2011; Sun et al. 2022). Collectively, three major clusters observed from the age spectrum

of the Benxi Formation are compatible with three major geologic events that built the North Qinling Terrane. In addition, a paucity of ca. 320–300 Ma age components fits well with an epoch of magmatic quiescence then.

For the Permian samples, a significant age population of ca. 1000–800 Ma is absent, but the age population of ca. 2000–1800 Ma is predominant (Fig. 8d). Lacking ages in the prolonged age span from ca. 1700 to 550 Ma is a robust signal indicating a North China Block basement source, which experienced a long period of magmatic lull at that stage, excepting for some mafic dikes and volcanic eruptions (Peng 2015). The North China Block is characterized by two Archean-Paleoproterozoic tectonic flare-ups of ca. 2600–2400 Ma and ca. 2000–1800 Ma (Zhao et al. 2012; Sun et al. 2024), which can be clearly viewed from those Permian sandstones. Some samples display major age peaks of ca. 290 Ma, corresponding well with the Permian magmatic flare-up that generated a large number of plutons and eruptions in the Inner Mongolia Continental Arc, the construction of which was induced by the southward subduction of the southern Paleo-Asian Ocean lithosphere (Xiao et al. 2003; Sun et al. 2024). Also, two major peaks at ca. 420 Ma and 290 Ma separated by a lull between them are consistent with two major tectonic fluctuations in these two stages (Sun et al. 2024). Therefore, we conclude sediment derivation of Permian succession from the Inner Mongolia Continental Arc, a Paleozoic Andes-type continental arc built upon the northern North China Block basement.

5.2 Implications for tectonic evolution of the northern North China Block margin

According to the calculated results, the Inner Mongolia Continental Arc crustal thickness thickened to about 60 km at ca. 440–400 Ma, then thinned to about 30–40 km during ca. 370–330 Ma (Fig. 10a). The inferred Late Ordovician crustal thickening event is synchronous with the accretion of the Bainaimiao Arc onto the northern North China Block (Sun and Dong 2020), while the subsequent crustal thinning can be attributed to post-collision extension along the northern North China Block (Sun et al. 2024). From ca. 295 Ma, the Inner Mongolia Continental Arc crust thickened continuously to about 60 km at ca. 280 Ma, consistent in error with 58 ± 11 km proposed by Song et al. (2023), and can be verified by a stage of magmatic flare-up and fold-thrust activity in the Inner Mongolia Continental Arc (Song et al. 2018). Rapid uplift and erosion of the Inner Mongolia Continental Arc can be viewed from the common appearance of basement components in the sedimentary rocks, represented by the dominance of ca. 2600–1800 Ma-aged detrital zircons (Figs. 7, 8) and the enrichment of high-grade metamorphic rock fragments in the southern North China Block (Fig. 5). In addition, samples of the Shihezi Formation contain a significant amount of older basement rocks, in comparison to the Shanxi Formation sandstone that consists of equal amounts of Paleozoic arc-derived zircons and Archean to Paleoproterozoic basement-derived zircons. This evidence accords with the reconstructed crustal thickness variation of the Inner Mongolia Continental Arc, as surface erosional response to structural uplift of the arc system. Phases of rapid crustal thickening and subsequent denudation of the Inner Mongolia Continental Arc were also identified by Ma et al. (2014), who also highlighted the dynamic relation with the southward subduction of the Paleo-Asian Ocean (Xiao et al. 2003). The approximately 15-km-thick upper crust was eroded, predominantly during the Permian–Triassic (Zhang et al. 2007), resulting in direct exposure of widespread high-grade basement complexes there and enrichment of sedimentary lithics in Permian–Middle Triassic sediments. Rapid exhumation of the Inner Mongolia Continental Arc sustained throughout the Carboniferous to Permian, in view of the presence of Devonian-Permian-aged detrital zircons and Proterozoic–Ordovician sedimentary gravels in sediments of each stage, consistent with our observations.

5.3 Implications for early-stage uplift history of the western Qinling-Dabie Orogen

The North Qinling Terrane crust obviously thickened from ca. 500 Ma, with peak thickness of ~ 70–80 km at ca. 440 Ma (Fig. 10b), reflecting arc lithospheric shortening in response to back-arc basin closure that resulted in collision between the North Qinling Terrane and southern North China Block at ca. 450 Ma (Dong et al. 2011, 2021; Sun et al. 2020, 2022). One result indicating ~ 45 km crust thickness at ca. 300 Ma coincided with Late Carboniferous transgression from Late Carboniferous (Chen et al. 1989; Yang et al. 2014b; Sun et al. 2020, 2024), although more data are needed to strengthen this assumption. This interpretation shows that the North Qinling Terrane has been evaluated to ~ 4 km at the mid-Paleozoic. We note that provenances of the Benxi Formation from the southern North China Block are rare, whereas those originating from the North Qinling Terrene in the further south are predominant. This insight indicates that the North Qinling Terrene was significantly high at the Late Carboniferous (Fig. 11a), concordant with the calculated paleo-evaluation conclusion. Furthermore, the sedimentary facies of the Benxi Formation are dominated by tidal flat successions, without input transported by river delta, hinting that the nearby southern North China Block was relative flat then. Hence, we conclude that the topography of the southern North China Block and North Qinling Terrane was relatively stable with low relief but was hindered from the marine system opening to the Proto-Tethys Ocean by the North Qinling highland.

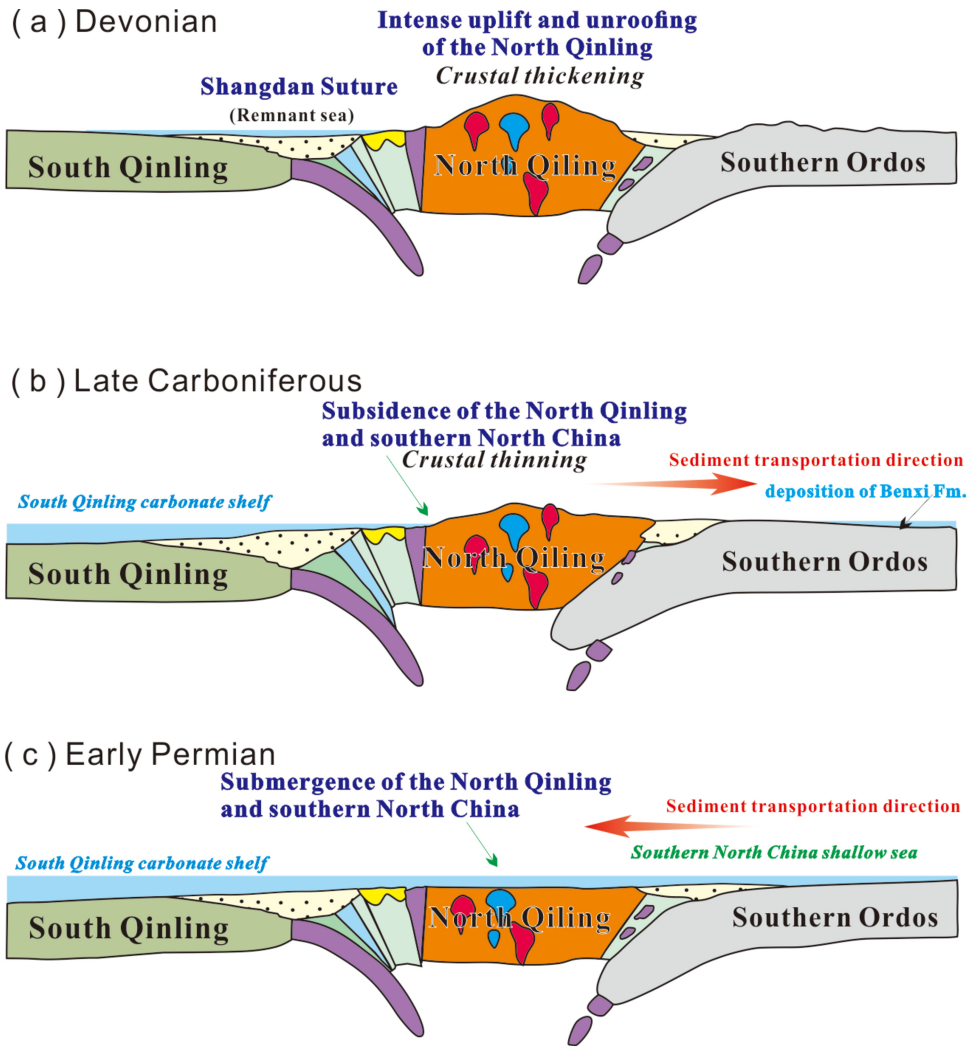

Fig. 11 Schematic tectonic model illustrating three stage changes in dynamic settings for the deposition and the provenance shift between the Ordos Basin and the Qinling Orogen

For the Early Permian stage, the North Qinling Terrane was submerged and flooded by a marine basin (Fig. 11b), above which deltaic associations covered the southern Ordos and the North Qinling Terrane (Yang et al. 2014b, 2016, 2021; Li et al. 2021a). A northerly source from the Inner Mongolia Continental Arc began to accumulate in the northern flank of the North Qinling Terrane, before termination approximately along the southern North Qinling Terrane, where shallow-water carbonate shelf sedimentation sustained from the Devonian to Triassic (Yang et al. 2021; Cheng et al. 2022). Hence, paleoflow data from the Shanxi and Shihezi Formations generally dip southward (Fig. 3a). This also leads to a new assumption that the proto-Ordos Basin was marine throughout the Late Carboniferous to Early Permian, being the continent ward part of a vast basin extending from the Inner Mongolia Continental Arc of the Paleo-Asian Ocean margin to the South Qinling carbonate shelf rim of the Paleo-Tethys Ocean rim (Fig. 11).

Collectively, our new interpretation further indicates that the North Qinling Terrane experienced a significant uplift history from ca. 500 Ma and remained as a relatively low-relief highland until end-Carboniferous. The Permian submergence of the North Qinling Terrane, covered by deltaic facies, indicates that uplift of the western Qinling-Dabie orogen lasted ~ 150 Ma after the Proto-Tethys Ocean closure.

6 Conclusions

The Late Carboniferous Benxi Formation was sourced from the south, where the North Qinling Terrane provided detritus mostly of Neoproterozoic and Early Paleozoic ages, with additional sources from the southern North China Block basement.

The Early Permian successions are dominated by Neoarchean, Paleoproterozoic, Early Paleozoic, and Late Paleozoic age populations, with an age gap between 1600 and 550 Ma, characterizing a sediment derivation from the Inner Mongolia Continental Arc.

The distinct sandstone petrologic compositions, detrital zircon U–Pb age patterns, and paleoflow shift from north- to south-directed jointly reveal a provenance shift at the Carboniferous-Permian transition.

The North Qinling Terrane experienced a significant uplift history from ca. 500 Ma and remained as a highland until end-Carboniferous, indicating that the uplift of the western Qinling-Dabie orogen lasted ~ 150 Ma after the Proto-Tethys Ocean closure.

Acknowledgements The authors would like to acknowledge editors and referees for insightful comments that led to a better version of our work. Financial support for this study was jointly given by the National Natural Science Foundation of China (Grant Nos: 42372253 and 42072260), the Youth Innovation Team of Shaanxi Universities, and the Science and Technology Project of PetroChina (No. 2023ZZ0201).

Author contributions CY: conceptualization, data curation, funding acquisition, investigation, methodology, writing–original draft, writing–review and editing; JS: conceptualization, funding acquisition, investigation, writing–original draft, writing–review and editing; ZL: investigation, writing–review and editing; YQ: investigation (supporting), writing–original draft; KY: investigation, writing–review and editing; JZ: investigation, writing–review and editing; ZW: investigation, writing–review and editing.

Data availability All related research data were uploaded as the supplementary materials.

Declarations

Conflict of interest The authors declare that they have no known competing financial interests or personal relationships that could have appeared to influence work reported in this paper.

References

Andersen T (2002) Correction of common lead in U-Pb analyses that do not report ^{204}Pb. Chem Geol 192(1–2):59–79. https://doi.org/10.1016/S0009-2541(02)00195-X

Belousova E, Griffin W, O'Reilly SY, Fisher N (2002) Igneous zircon: trace element composition as an indicator of source rock type. Contrib Mineral Petrol 143(5):602–622. https://doi.org/10.1007/s00410-002-0364-7

Black LP, Kamo SL, Allen CM, Aleinikoff JN, Davis DW, Korsch RJ, Foudoulis C (2003) TEMORA 1: a new zircon standard for Phanerozoic U–Pb geochronology. Chem Geol 200(1–2):155–170. https://doi.org/10.1016/S0009-2541(03)00165-7

Chen ZH, Zhang NM, Zhang SL, Ma JX, Wu FD (1989) The time and spatial evolution of sedimentary systems and coal-accumulating centre in Late Palaeozoic coal-bearing measures on the eastern margin of Ordos basin. Earth Sci 14(4):357–366 (**in Chinese with English abstract**)

Cheng C, Li SY, Xie XY, Shen YF, Ying PL, Manger WL, Cao TL (2022) Sedimentary evolution and sea-level fluctuation of a Paleo-Tethyan Permian carbonate-dominated succession from Central China. Sediment Geol 440:106244. https://doi.org/10.1016/j.sedgeo.2022.106244

Dickinson WR (1985) Interpreting provenance relations from detrital modes of sandstones. In: Zuffa GG (ed) Provenance of arenites. Springer, Dordrecht, pp 333–361

Dickinson WR, Suczek CA (1979) Plate tectonics and sandstone compositions. AAPG Bull 63:2164–2182. https://doi.org/10.1306/2f9188fb-16ce-11d7-8645000102c1865d

Dong YP, Santosh M (2016) Tectonic architecture and multiple orogeny of the Qinling Orogenic Belt, Central China. Gondwana Res 29(1):1–40. https://doi.org/10.1016/j.gr.2015.06.009

Dong YP, Zhang GW, Neubauer F, Liu XM, Genser J, Hauzenberger C (2011) Tectonic evolution of the Qinling Orogen, China: review and synthesis. J Asian Earth Sci 41(3):213–237. https://doi.org/10.1016/j.jseaes.2011.03.002

Dong YP, Liu XM, Zhang GW, Chen Q, Zhang XN, Li W, Yang C (2012) Triassic diorites and granitoids in the Foping area: constraints on the conversion from subduction to collision in the Qinling Orogen, China. J Asian Earth Sci 47:123–142. https://doi.org/10.1016/j.jseaes.2011.06.005

Dong YP, Neubauer F, Genser J, Sun SS, Yang Z, Zhang FF, Cheng B, Liu XM, Zhang GW (2018) Timing of orogenic exhumation processes of the Qinling Orogen: evidence from ^{40}Ar/^{39}Ar dating. Tectonics 37:4037–4067. https://doi.org/10.1029/2017TC004765

Dong YP, Sun SS, Santosh M, Zhao J, Sun JP, He DF, Shi XH, Hui B, Cheng C, Zhang GW (2021) Central China Orogenic Belt and amalgamation of East Asian continents. Gondwana Res 100:131–194. https://doi.org/10.1016/j.gr.2021.03.006

Guo YQ, Li WH, Guo BC, Zhang Q, Chen Q, Wang RG, Liu X, Mao Y, Li ZC, Zhang MT, Li BQ (2019) Sedimentary systems and palaeogeography evolution of Ordos Basin. J Palaeogeogr 21(2):293–320 (**in Chinese with English abstract**)

Hawkesworth CJ, Kemp AIS (2006) Using hafnium and oxygen isotopes in zircons to unravel the record of crustal evolution. Chem Geol 226(3–4):144–162. https://doi.org/10.1016/j.chemgeo.2005.09.018

Huang BC, Yan YG, Piper JDA, Zhang DH, Yi ZY, Yu S, Zhou TH (2018) Paleomagnetic constraints on the paleogeography of the east Asian blocks during Late Paleozoic and early Mesozoic times. Earth Sci Rev 186:8–36. https://doi.org/10.1016/j.earscirev.2018.02.004

Li WH, Chen Q, Li ZC, Wang RG, Wang Y, Ma Y (2012) Lithofacies palaeogeography of the early Paleozoic in Ordos area. J Palaeogeogr 14(1):85–100 (**in Chinese with English abstract**)

Li Y, Fan AP, Yang RC, Sun YP, Lenhardt N (2021a) Sedimentary facies control on sandstone reservoir properties: a case study from the Permian Shanxi Formation in the southern Ordos Basin, Central China. Mar Petrol Geol 129:105–183. https://doi.org/10.1016/j.marpetgeo.2021.105083

Li WH, Zhang Q, Li KY, Chen Q, Guo YQ, Ma Y, Feng JP, Zhang DF (2021b) Sedimentary evolution of the Late Paleozoic in Ordos Basin and its adjacent areas. J Palaeogeogr 23(01):39–52 (**in Chinese with English abstract**). https://doi.org/10.7605/gdlxb.2021.01.003

Li Y, Fan AP, Yang RC, Sun YP, Lenhardt N (2022) Braided deltas and diagenetic control on tight sandstone reservoirs: a case study on the Permian Lower Shihezi Formation in the southern Ordos Basin (Central China). Sediment Geol 435:106156. https://doi.org/10.1016/j.sedgeo.2022.106156

Li LX, Gu T, Gong HJ, Chi RL, Liu T (2023) Determination of the top boundary strata of the Taiyuan Formation in the Southeastern Ordos Basin-Constrained by U-Pb geochronology of the Shanxi Formation-Taiyuan Formation in the Yichuan Area. Acta Sediment Sinica (**in Chinese with English abstract**). https://doi.org/10.14027/j.issn.1000-0550.2023.137

Liu XM, Gao S, Diwu CR, Yuan HL, Hu ZC (2007) Simultaneous *in-situ* determination of U-Pb age and trace elements in zircon

by LA–ICP–MS in 20 μm spot size. Chin Sci Bull 52(9):1257–1264. https://doi.org/10.1007/s11434-007-0160-x

Liu CY, Zhao HG, Sun YZ (2009) Tectonic background of Ordos basin and its controlling role for basin evolution and energy mineral deposits. Energy Explor & Exploit 27(1):15–27. https://doi.org/10.1260/014459809788708219

Liu CY, Wang JQ, Zhao HG, Zhang DD, Zhao XC (2015) The classification of sedimentary basins and discussion on relevant issues. Earth Sci Front 22:1–26 (**in Chinese with English abstract**). https://doi.org/10.13745/j.esf.2015.03.001

Liu L, Liu LJ, Xu YG (2021) Mesozoic intraplate tectonism of East Asia due to flat subduction of a composite terrane slab. Earth Sci Rev 214:103505. https://doi.org/10.1016/j.earscirev.2021.103505

Ludwig KR (2003) User's manual for IsoPlot 3.0. A geochronological toolkit for Microsoft 2003 Excel 71.

Ma SX, Meng QR, Duan L, Wu GL (2014) Reconstructing Late Paleozoic exhumation history of the Inner Mongolia Highland along the northern edge of the North China Craton. J Asian Earth Sci 87:89–101. https://doi.org/10.1016/j.jseaes.2014.02.020

Meng QR, Wu GL, Fan LG, Wei HH (2019) Tectonic evolution of early Mesozoic sedimentary basins in the North China block. Earth Sci Rev 190:416–438. https://doi.org/10.1016/j.earscirev.2018.12.003

Peng P (2015) Late Paleoproterozoic-Neoproterozoic (1800–541 Ma) mafic dyke swarms and rifts in North China. In: Zhai M (ed) Precambrian Geology of China. Springer, Berlin, pp 171–204. https://doi.org/10.1007/978-3-662-47885-1_4

Peng YX, Guo SB (2023) Lithofacies analysis and paleosedimentary evolution of Taiyuan Formation in southern North China basin. J Petrol Sci Eng 220:111127. https://doi.org/10.1016/j.petrol.2022.111127

Pettijohn FJ (1975) Sedimentary Rocks, 3rd edn. Harper and Row, New York

Qian T, Liu SF, Li WP, Gao TJ, Chen XL (2015) Early-Middle Jurassic evolution of the northern Yangtze foreland basin: a record of uplift following Triassic continent–continent collision to form the Qinling-Dabieshan orogenic belt. Int Geol Rev 57(3):327–341. https://doi.org/10.1080/00206814.2015.1006270

Richards JP (2015) Tectonic, magmatic, and metallogenic evolution of the Tethyan orogen: from subduction to collision. Ore Geol Rev 70:323–345. https://doi.org/10.1016/j.oregeorev.2014.11.009

Shao LY, Yang ZY, Shang XX, Xiao ZH, Wang S, Zhang WL, Zheng MQ, Lu J (2015) Lithofacies Palaeogeography of the Carboniferous and Permian in the Qinshui basin, Shanxi Province. China J Palaeogeogr 4(4):384–412. https://doi.org/10.1016/j.jop.2015.06.001

Shen BH, Shen SZ, Wu Q, Zhang SC, Zhang B, Wang XD, Hou ZS, Yuan DX, Zhang YC, Liu F, Liu J, Zhang H, Shi YK, Wang J, Feng Z (2022) Carboniferous and Permian integrative stratigraphy and timescale of North China Block. Sci China Earth Sci 65(6):983–1011. https://doi.org/10.1007/s11430-021-9909-9

Song SG, Bi HZ, Qi SS, Yang LM, Allen MB, Niu YL, Su L, Li WF (2018) HP-UHP metamorphic belt in the east Kunlun Orogen: final closure of the Proto-Tethys Ocean and formation of the Pan-North-China Continent. J Petrology 59(11):2043–2060. https://doi.org/10.1093/petrology/egy089

Song DF, Mitchell RN, Xiao WJ, Mao QG, Wan B, Ao SJ (2023) Andean-type orogenic plateau as a trigger for aridification in the arcs of northeast Pangaea. Commun Earth Environ 4:306. https://doi.org/10.1038/s43247-023-00976-2

Sun JP, Dong YP (2019) Cambrian tectonic evolution of the northwestern Ordos terrane, North China: constraints of stratigraphy, sedimentology and zircon U-Pb geochronology. Int J Earth Sci 108(2):569–586. https://doi.org/10.1007/s00531-018-1669-8

Sun JP, Dong YP (2020) Ordovician tectonic shift in the western North China Craton constrained by stratigraphic and geochronological analyses. Basin Res 32(6):1413–1440. https://doi.org/10.1111/bre.12435

Sun JP, Yang L, Dong YP, Yang XY, Peng Y, Zhao J (2020) Permian tectonic evolution of the southwestern Ordos Basin, North China: integrating constraints from sandstone petrology and detrital zircon geochronology. Geol J 55(12):8068–8091. https://doi.org/10.1002/gj.3916

Sun JP, Dong YP, Chen Q, Yang L, Li WH, Zhang DD, Zhang Q (2022) Ordovician tectonic transition from passive margin into peripheral foreland in the southern Ordos: a diagnostic insight into the closure of Erlangping Ocean between the North Qinling Arc and North China Block. Basin Res 35(1):336–362. https://doi.org/10.1111/bre.12714

Sun JP, Dong YP, Chen Q, Ma Y (2024) Revisiting Ediacaran to Early Cambrian depositional history of western North China: Did it remain passive until the Mid-Paleozoic? J Geol Soc 181(2):jgs2023–jgs2150. https://doi.org/10.1144/jgs2023-150

Sun FY (2019) Study on provenance and aluminum enrichment of the Benxi Formation in the southeastern part of North China Block (PhD thesis). Henan Polytechnic University

Tang M, Ji WQ, Chu X, Wu AB, Chen C (2021) Reconstructing crustal thickness evolution from europium anomalies in detrital zircons. Geology 49(1):76–80. https://doi.org/10.1130/g47745.1

Wang ZZ, Han BF, Feng LX, Liu B (2015) Geochronology, geochemistry and origins of the Paleozoic–Triassic plutons in the Langshan area, western Inner Mongolia, China. J Asian Earth Sci 97:337–351. https://doi.org/10.1016/j.jseaes.2014.08.005

Wang X, Liu XS, Zhao WB, Zhang L, Hu JL, Tian JC, Chen R, Wang J, Wu JY, Xiao YW (2023) Detrital zircon U-Pb geochronology characteristics of Permian sandstone and its constraints on the tectonic evolution of the southern Ordos Basin. Acta Sediment Sinica 41:1396–1413 (**in Chinese with English abstract**). https://doi.org/10.14027/j.issn.1000-0550.2022.118

Wu P, Wu YB, Zhou GY, Zhang WX, He Y (2021) Geochronology, geochemistry, and isotope compositions of "Grenvillian" S-type granites in the North Qinling unit, Central China: Petrogenesis and tectonic significance. Precambrian Res 360:106247. https://doi.org/10.1016/j.precamres.2021.106247

Xiao WJ, Windley BF, Hao J, Zhai MG (2003) Accretion leading to collision and the Permian Solonker suture, Inner Mongolia, China: termination of the Central Asian Orogenic Belt. Tectonics 22(6):1069. https://doi.org/10.1029/2002TC001484

Xiao WJ, Windley BF, Sun S, Li JL, Huang BC, Han CM, Yuan C, Sun M, Chen HL (2015) A tale of amalgamation of three Permo-Triassic collage systems in central Asia: Oroclines, sutures, and terminal accretion. Annu Rev Earth Planet Sci 43:477–507. https://doi.org/10.1146/annurev-earth-060614-105254

Yang WT, Yang JH, Wang XF, Du YS (2014a) Uplift-denudation history of the Qinling Orogen: constrained from the detrital-zircon U-Pb geochronology. J Asian Earth Sci 89:54–65. https://doi.org/10.1016/j.jseaes.2014.03.025

Yang JH, Cawood PA, Du Y, Feng B, Yan JX (2014b) Global continental weathering trends across the Early Permian glacial to postglacial transition: correlating high- and low-paleolatitude sedimentary records. Geology 42(10):835–838. https://doi.org/10.1130/G35892.1

Yang M, Liu L, Wang YW, Liao XY, Kang L, Gai YS (2016) Geochronology of detrital zircons from metaclastic of Erlangping complex in the North Qinling belt and its tectonic implication. Acta Petrol Sin 32(5):1452–1466 (**in Chinese with English abstract**)

Yang WT, Wang M, Zheng DS, Du YS (2018) Late Triassic sedimentary record from the Nanzhao Basin and implications for the orogeny in the Qinling Orogenic Belt, Central China. J Asian Earth Sci 166:120–135. https://doi.org/10.1016/j.jseaes.2018.07.038

Yang JH, Cawood PA, Montañez IP, Condon DJ, Du YS, Yan JX, Yan SQ, Yuan DX (2020) Enhanced continental weathering and large

igneous province induced climate warming at the Permo-Carboniferous transition. Earth Planet Sci Lett 534:116074. https://doi.org/10.1016/j.epsl.2020.116074

Yang WT, Peng SY, Wang M, Zhang HY (2021) Provenance of upper Permian-Triassic sediments in the south of North China: implications for the Qinling orogeny and basin evolution. Sediment Geol 424:106002. https://doi.org/10.1016/j.sedgeo.2021.106002

Yu ZP, Meng QR (1995) Late Paleozoic sedimentary and tectonic evolution of the Shangdan suture zone, Eastern Qinling, China. J Southeast Asian Earth Sci 11(3):237–242. https://doi.org/10.1016/0743-9547(95)98084-F

Yu XH, Wang XZ, Wang NX, Shan X, Zhou JS, Han XQ, Li YL, Du YH, Zhao CF (2017) Sequence stratigraphic framework and sedimentary evolution characteristics of gas-bearing sandbody in the Upper Paleozoic in southeastern Ordos Basin. J Palaeogeogr 19:935–954 (**in Chinese with English abstract**). https://doi.org/10.7605/gdlxb.2017.06.073

Zhang XX (2020) Source-sink analysis and tectonic paleogeographic significance of Benxi for Mation in the southern Ordos Basin (Master's thesis). Chengdu University of Technology (**in Chinese with English Abstract**) https://doi.org/10.26986/d.cnki.gcdlc.2020.001217

Zhang GW, Zhang BR, Yuan XC, Xiao QH (2001) Qinling orogenic belt and continental dynamics. Science Press, Beijing

Zhang SH, Zhao Y, Liu J, Hu JM, Chen Z, Li M, Pei JL, Chen ZY, Zhou JX (2007) Emplacement depths of the Late Paleozoic-Mesozoic granitoid intrusions from the northern North China block and their tectonic implications. Acta Petrol Sin 23(3):625–638 (**in Chinese with English abstract**). https://doi.org/10.3969/j.issn.1000-0569.2007.03.010

Zhang J, Zhang BH, Zhao H (2016a) Timing of amalgamation of the Alxa Block and the North China Block: Constraints based on detrital zircon U-Pb ages and sedimentologic and structural evidence. Tectonophysics 668:65–81. https://doi.org/10.1016/j.tecto.2015.12.006

Zhang SH, Zhao Y, Liu JM, Hu ZC (2016b) Different sources involved in generation of continental arc volcanism: the Carboniferous-Permian volcanic rocks in the northern margin of the North China block. Lithos 240:382–401. https://doi.org/10.1016/j.lithos.2015.11.027

Zhao GC, Cawood PA, Li SZ, Wilde SA, Sun M, Zhang J, He YH, Yin CQ (2012) Amalgamation of the North China Craton: key issues and discussion. Precambrian Res 222–223:55–76. https://doi.org/10.1016/j.precamres.2012.09.016

Zhao GC, Wang YJ, Huang BC, Dong YP, Li SZ, Zhang GW, Yu S (2018) Geological reconstructions of the east Asian blocks: from the breakup of Rodinia to the assembly of Pangea. Earth Sci Rev 186:262–286. https://doi.org/10.1016/j.earscirev.2018.10.003

Zhu HT, Chen KY, Liu KY, He S (2008) A sequence stratigraphic model for reservoir sand-body distribution in the Lower Permian Shanxi Formation in the Ordos Basin, northern China. Mar Petrol Geol 25(8):731–743. https://doi.org/10.1016/j.marpetgeo.2008.03.007